A&A 617, A21 (2018)
https://doi.org/10.1051/0004-6361/201832792

Astronomy & Astrophysics

Hot prominence detected in the core of a coronal mass ejection

III. Plasma filling factor from UVCS Lyman-α and Lyman-β observations

R. Susino[1], A. Bemporad[1], S. Jejčič[2,3], and P. Heinzel[3]

[1] INAF – Turin Astrophysical Observatory, 10025 Pino Torinese (TO), Italy
e-mail: susino@oato.inaf.it
[2] Faculty of Mathematics and Physics, University of Ljubljana, 1000 Ljubljana, Slovenia
[3] Astronomical Institute, The Czech Academy of Sciences, 25165 Ondřejov, Czech Republic

Received 8 February 2018 / Accepted 28 May 2018

ABSTRACT

Context. We study an erupting prominence embedded in the core of a coronal mass ejection that occurred on August 2, 2000, and focus on deriving the plasma filling factor of the prominence.
Aims. We explore two methods for measuring this factor along the line of sight. They are based on a combination of visible-light and ultraviolet spectroscopic observations.
Methods. Theoretical relationships for resonant scattering and collisional excitation were used to evaluate the intensity of the neutral hydrogen Lyman-α and Lyman-β lines in two prominence points where simultaneous and cospatial LASCO-C2 and UVCS data were available. Thermodynamic and geometrical parameters assumed for the calculation (i.e., electron column density, kinetic temperature, flow velocity, chromospheric Lyα and Lyβ intensities and profiles, and thickness of the prominence along the line of sight) are provided by both observations and the results of a detailed 1D non-local thermal equilibrium (non-LTE) radiative-transfer model of the prominence, developed in our previous work. The geometrical filling factor was derived from comparing the calculated and measured intensities of the two lines. The results were then checked against the non-LTE model in order to verify the reliability of the methods.
Results. The resulting filling factors are consistent with the model in both prominence points when the radiative and collisional components of the total intensity of the hydrogen lines are separated using the Lyα and Lyβ line intensities, which is required to estimate the filling factor. The exploration of the parameter space shows that the results are weakly sensitive to the plasma flow velocity, but depend more strongly on the assumed kinetic temperatures.
Conclusions. The combination of visible-light and ultraviolet Lyα and Lyβ data can be used to approximately estimate the line-of-sight geometrical filling factor in erupting prominences, but the proposed technique, which is model dependent, is reliable only for emission that is optically thin in the lines considered, a condition that is not in general representative of prominence plasma.

Key words. Sun: corona – Sun: filaments, prominences – Sun: coronal mass ejections – Sun: UV radiation

1. Introduction

Prominences are underlying structures of the solar atmosphere that consist of cool and dense plasma (typically at temperatures of $\sim 10^4$ K and densities of $\sim 10^{11}$ cm^{-3}), which is sustained against the solar gravity by the magnetic field. They are thought to consist of chromospheric gas entrapped in magnetic flux ropes anchored on the solar surface (see Mackay et al. 2010; Labrosse et al. 2010; Vial & Engvold 2015, for a comprehensive overview of solar prominences). They can eventually erupt as a result of magnetic instabilities that trigger coronal mass ejections (CMEs; see Chen 2011; Webb & Howard 2012), and then appear as the bright core of these structures in visible-light images acquired by coronagraphs (e.g., Akmal et al. 2001; Ciaravella et al. 2003).

Observations, carried out in particular in the ultraviolet wavelength domain (see, e.g., Patsourakos & Vial 2002, for a review of SOHO prominence observations), have provided evidence that they consist of small-scale, elongated threads and fine structures filling only a small fraction of the prominence volume (e.g., Berger 2014). Thermodynamic modeling of prominences, which is based on the measured emission, critically depends on the proper knowledge of the real volume filled by the radiating plasma (Labrosse et al. 2010; Labrosse 2015). The filling factor is the crucial parameter that gives a measure of the effective emitting volume, and it therefore is fundamental for a correct interpretation of observed line emission.

There are several definitions of filling factor and many ways to measure it (see the discussion in Labrosse et al. 2010). For the optically thin emission coming from the transition-region envelope of prominences (the so-called PCTR; see Parenti 2015), the most common approach is to divide the inferred emission measure by the square of the electron density, derived from the ratio of density-sensitive lines, and compare the result with the prominence size estimated from observations (see, e.g., Mariska et al. 1979). Resulting filling factors are on the order of a few percents (up to ~0.03; see, e.g., Labrosse et al. 2010) and suggest highly inhomogeneous density distributions. The cool counterpart of the prominence can be more structured than the PCTR, implying even lower values of the filling factor.

An alternative method that can be used to estimate this parameter is based on the ratio of the intensity of a collisionally excited emission line to the square of the visible-light polarized brightness (pB). This approach was used by Fineschi & Romoli (1994) and Romoli & Fineschi (1994) to derive the coronal irregularity factor (which is proportional to the reciprocal of the filling

factor; see Allen 1963) from the relative intensities of the neutral hydrogen Lyman-α and Lyman-β emission lines for several coronal structures.

In this work we explore a similar technique, showing that an estimate of the filling factor can be obtained from simultaneous and cospatial visible-light and ultraviolet observations of an erupting prominence embedded in the core of a CME. This event has been studied in some previous papers (Heinzel et al. 2016; Jejčič et al. 2017; hereafter Paper I and Paper II, respectively), where SOHO/LASCO-C2 and SOHO/UVCS data were used to constrain a thermodynamic model of the prominence structure. In comparison with standard quiescent prominences, this prominence was found to be relatively hot and tenuous (with a temperature of $\sim 10^5$ K and an electron density of $\sim 10^8$ cm^{-3}) because it expanded at quite high velocities. In the present analysis, we exploit UVCS and LASCO-C2 visible-light observations, as well as the modeling results, to test this alternative way to infer the prominence plasma filling factor.

The paper is organized as follows: in Sect. 2 we recall the theoretical formulation of resonant scattering and collisional excitation of coronal neutral hydrogen Lyman lines; in Sect. 3 we summarize the observational and modeling results obtained in Paper I; we then describe the analysis methods and results in Sects. 4 and 5, and discuss them in Sect. 6.

2. Basic theory of UV line formation

Under typical coronal conditions, the upper levels of the neutral hydrogen Lyα and Lyβ transitions are populated mainly through the mechanisms of photon absorption and collisional excitation and are depopulated by spontaneous emission toward the ground level. Therefore, the total integrated intensity in the lines is a mixture of radiative (i.e., produced by resonant scattering) and collisional components:

$$I_{\rm tot} = I_{\rm rad} + I_{\rm col}. \tag{1}$$

According to Noci et al. (1987), the radiative component is given by

$$I_{\rm rad} = B_{ij}\, h\lambda_{ij} \frac{b_{ij}}{4\pi} \int_{\rm LOS} n_i \int_{\Omega} p(\phi) F(\delta\lambda)\, {\rm d}\omega\, {\rm d}l, \tag{2}$$

where B_{ij} is the Einstein coefficient for photon absorption from the ground level i to the excited level j (in units of sr cm^2 erg^{-1} s^{-1}), h the Planck constant, λ_{ij} the rest wavelength of the transition, b_{ij} the branching fraction for de-excitation ($b_{12} = 1$ for Lyα and $b_{13} \simeq 0.88$ for Lyβ), n_i the number density of hydrogen atoms in the ground level, Ω the solid angle subtended by the incident radiation source, $p(\phi)$ gives the angular dependence of the scattering process, and

$$F(\delta\lambda) = \int_0^{\infty} I_{\odot}(\lambda - \delta\lambda)\Phi(\lambda)\, {\rm d}\lambda, \tag{3}$$

is the so-called Doppler-dimming factor, which accounts for the velocity-dependent irradiation and depends on the Doppler shift of the incident radiation as seen by the scattering atom moving with velocity v along the direction of illumination, $\delta\lambda = \lambda_{ij} v/c$, the spectral profile of the incident radiation, $I_{\odot}(\lambda)$ (in units of erg cm^{-2} s^{-1} sr^{-1} Å^{-1}), and the normalized absorption profile, $\Phi(\lambda)$. If the velocity distribution of the scattering atoms is Maxwellian, the absorption profile is Gaussian, with a Doppler width given by

$$\Delta\lambda_{\rm D} = \frac{\lambda_{ij}}{c}\sqrt{\frac{2k_{\rm B}T}{m}}, \tag{4}$$

where $k_{\rm B}$ is the Boltzmann constant, T is the kinetic (or ion) temperature, and m is the atomic mass. However, nonthermal motions, such as bulk expansion and turbulence, can broaden the absorption profile and increase the effective observed plasma temperature so that $T_{\rm eff} = T + m\xi^2/(2k_{\rm B})$, where ξ is the Gaussian-distributed nonthermal velocity.

For a low-density coronal plasma, the number density of hydrogen atoms in the ground level can be approximated in the following way:

$$n_i \approx n_{\rm H} \approx 0.83\, R(T)\, n_{\rm e}, \tag{5}$$

where $n_{\rm H}$ is the number density of neutral hydrogen, the factor 0.83 is the ratio between proton and electron density for a fully ionized gas with 10% helium, and $R(T)$ is the hydrogen ionization fraction at temperature T.

In Eq. (2), integration is performed along the line of sight (LOS) across the entire corona. However, when the emitting plasma is confined in a small region where all the thermodynamic quantities can be reasonably considered uniform and approximated by their mean values, and the contribution from the surrounding corona can be neglected, using Eq. (5), the radiative component can be simplified as

$$I_{\rm rad} \approx B_{ij}\, h\lambda_{ij} \frac{b_{ij}}{4\pi} \cdot \frac{\langle\Omega\rangle}{4\pi} F(\langle w\rangle) \cdot 0.83\, R(\langle T\rangle)\langle n_{\rm e}\rangle \cdot D_{\rm eff}, \tag{6}$$

where $D_{\rm eff}$ is the effective length of the LOS section across the emitting plasma volume, and the brackets denote LOS-averaged values. The factor $\langle\Omega\rangle/4\pi$ is the dilution factor.

The collisional component has the following form:

$$I_{\rm col} = \frac{hc}{\lambda_{ij}} \frac{b_{ij}}{4\pi} \int_{\rm LOS} n_i\, q_{ij}(T)\, n_{\rm e}\, {\rm d}l, \tag{7}$$

where $q_{ij}(T)\cdot n_{\rm e}$ is the collisional emission rate coefficient at temperature T. With the same considerations as above, the previous expression can be approximated as

$$I_{\rm col} \approx \frac{hc}{\lambda_{ij}} \frac{b_{ij}}{4\pi} \cdot q_{ij}(\langle T\rangle) \cdot 0.83\, R(\langle T\rangle)\langle n_{\rm e}^2\rangle \cdot D_{\rm eff}. \tag{8}$$

Introducing the electron column density $N_{\rm e} \approx \langle n_{\rm e}\rangle \cdot D_{\rm eff}$, giving the total number of electrons per unit area along the LOS, and the irregularity factor $X \equiv \langle n_{\rm e}^2\rangle/\langle n_{\rm e}\rangle^2$, giving a measure of the inhomogeneity of the coronal electron density distribution (Fineschi & Romoli 1994), it follows that $I_{\rm rad} \propto N_{\rm e}$ and $I_{\rm col} \propto N_{\rm e}^2 \cdot X/D_{\rm eff}$. Since the effective thickness of the emitting plasma along the LOS and the irregularity factor are usually unknown, all information about the LOS plasma distribution can be conveniently enclosed in the so-called filling factor f, which is defined so that

$$D_{\rm eff} = D \cdot X \cdot f, \tag{9}$$

where the length D is the apparent thickness of the emitting feature. In this way, it is possible to account for inhomogeneities of the coronal electron-density distribution and potential fragmentations of the plasma along the LOS, since f gives a measure of the real fraction of the LOS filled with the plasma emitting the observed spectral lines if D is over/underestimated. We note that filling factor calculations typically assume that the emitting plasma consists of material of uniform density surrounded by empty space, which is a simplification implying $X \approx 1$ (see Labrosse et al. 2010). We also note that of the two intensity components mentioned above, only the collisional one explicitly depends on the filling factor through its dependence on effective thickness and on the irregularity factor.

Combination of Eqs. (6), (8), and (9) can be used to derive the filling factor from the observed intensities of the hydrogen Lyα and Lyβ lines if the electron column density is measured, for instance, from visible-light data:

$$f = K(T) \cdot \frac{N_e^2}{I_{col} \cdot D} = K(T) \cdot \frac{N_e^2}{(I_{tot} - I_{rad}) \cdot D}, \quad (10)$$

where

$$K(T) = \frac{hc}{\lambda_{ij}} \frac{b_{ij}}{4\pi} \cdot q_{ij}(\langle T \rangle) \cdot 0.83\, R(\langle T \rangle) \quad (11)$$

depends on the average kinetic temperature and the other atomic parameters.

We finally emphasize that with the approximations used in the above relationships, all the measured and derived quantities must be regarded as LOS-weighted averages; moreover, each term in the equations (Doppler-dimming coefficient, collisional rates, hydrogen ionization fraction, etc.) has a different weighting with electron density, temperature, and flow velocity, thus they may be representative of different parts of the emitting structure if the distribution of the plasma parameters along the LOS is not actually uniform.

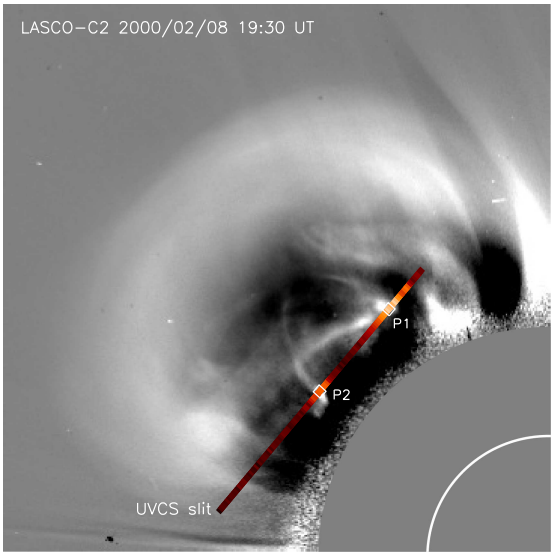

Fig. 1. LASCO-C2 mass image acquired at 19:30 UT on August 2, 2000, and intensity distribution of the Lyα line along the UVCS slit (measured at the same time and represented with color gradient). The two points considered in this analysis (P1, located at a helio-latitude of ~57° N, and P2, located at ~37° N) are also indicated.

3. Prominence observations and modeling results

In Paper I we presented observations of an erupting prominence in the core of a CME that occurred on August 2, 2000. We refer to Paper I and Paper II for a detailed description of the event. The prominence was observed in the visible light by the LASCO-C2 coronagraph and in the UV by the UVCS spectro-coronagraph, both on board the SOHO spacecraft.

Total-brightness LASCO images were used to infer the electron column density N_e of the CME and prominence plasma by applying the method described in Vourlidas et al. (2000) to the so-called "excess-brightness" image of the CME (see Fig. 1), obtained by subtracting the pre-event frame acquired at 16:04 UT from the LASCO-C2 frame containing the CME at 19:30 UT. LASCO images were also used to measure the plane-of-the-sky (POS) velocity of the prominence, $v_{POS} \simeq 300$ km s^{-1}, as well as its projected thickness, $D \simeq 56\,000$ km, which was taken as an approximation of the prominence average LOS thickness, under the simple assumption of cylindrical geometry.

UVCS recorded spectra of several UV coronal lines (see Table 1 of Paper I for a complete list) as the prominence crossed its field of view (FOV), a 40 arcmin long slit placed perpendicularly to the solar radius at a latitude of 40°NE and heliocentric distance of 2.3 $R_\odot$ (see Fig. 1). In particular, spectral profiles of the neutral hydrogen Lyman-α (λ_{12} = 1215.67 Å) and Lyman-β (λ_{13} = 1025.72 Å) lines were acquired with a spatial resolution of 21 arcsec (≈15 000 km) and an integration time of 120 s during the entire CME event. Both lines systematically appear to be the superposition of two components with different widths, the narrower one representing, in our interpretation, real prominence emission, while the broader one is more likely due to plasma in the PCTR or, alternatively, in the hot plasma shroud surrounding the prominence (see Habbal et al. 2010).

The two components were separated with a double Gaussian fit to the line profiles, and consistency of the fit was verified with a minimum chi-squared analysis (see Paper I). A mean pre-event spectrum, obtained by averaging over several exposures preceding the onset of the eruption, was subtracted from the line profiles in order to remove the contribution from the quiet corona surrounding the prominence from the observed emission. This correction may not be accurate because, as evidenced by the depleted (black) region around the prominence in Fig. 1, much of the pre-event corona has been blown away by the CME during the eruption. However, prominences are generally very bright in the Lyman lines (e.g., Ciaravella et al. 2003), and the quiet-corona contribution can be assumed to be very small; therefore possible uncertainties related to the background subtraction can be considered negligible in this case.

Figure 2 reports the total integrated intensities of the Lyα and Lyβ narrow components as functions of time and position along the UVCS slit. The prominence exhibits a complex structure in both lines, with ramifications and apparently superimposed emission features. The intensity of the Lyα line is up to 250 times higher than that of the Lyβ. The Lyα to Lyβ intensity ratio is consistent with the value somewhat lower than ~500 measured by Ciaravella et al. (2003) in the prominence core of a CME observed with UVCS at an altitude of 2.3 $R_\odot$. Effective temperatures and Doppler shifts derived from the two line profiles, not shown here, outline the same scenario as described in Paper I: the prominence appears to be almost uniform in temperature ($T_{eff} \approx 10^5$ K), while striking differences in the LOS speeds characterize the two prominence legs, the southern leg moving towards the observer at a significantly higher velocity ($v_{LOS} \approx 300$ km s^{-1}) than the northern leg, which in contrast seems to remain anchored to the solar surface or to be slowly moving ($v_{LOS} \approx 25$ km s^{-1}).

The observational quantities derived from visible-light and UV data were used in Paper I to constrain a non-local thermal equilibrium (non-LTE; i.e., departures from local thermodynamic equilibrium) radiative-transfer model of the prominence, which provided us with all the other thermodynamic plasma parameters, such as the gas pressure, kinetic temperature, microturbulent velocity, ionization degree, and line opacity. The full non-LTE multilevel radiative-transfer problem was solved by means of a 1D numerical code (see Paper I for more details) for a set of prominence pixels, and in particular, for the two sole points along the prominence where simultaneous and cospatial

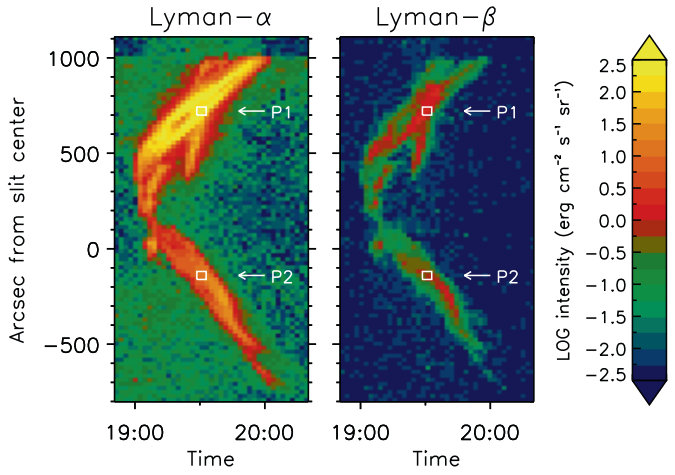

Fig. 2. Intensity distribution of the narrow component of the prominence Lyα and Lyβ lines, plotted as a function of time and position along the UVCS slit. 1 arcsec ≃ 800 km.

Table 1. Observed quantities and modeling results.

	P1	P2
Heliocentric distance ($R_\odot$)	2.46	2.35
N_e (10^{17} cm^{-2})	1.48 ± 0.03	0.39 ± 0.02
$I^{(\alpha)}$ (erg cm^{-2} s^{-1} sr^{-1})	216 ± 1	12.5 ± 0.8
$I^{(\beta)}$ (erg cm^{-2} s^{-1} sr^{-1})	0.9 ± 0.3	0.4 ± 0.1
$T_{\rm eff}$ (10^4 K)	10.9 ± 0.1	8.7 ± 0.8
$v_{\rm LOS}$ (km s^{-1})	24.6 ± 0.3	297 ± 2
$v_{\rm POS}$ (km s^{-1})	280 ± 30	
p (10^{-3} dyn cm^{-2})	0.52	2.1
n_e (10^8 cm^{-3})	0.36	1.1
T (10^4 K)	4.96	6.67
$T_{\rm eff}$ (10^4 K)	6.50	8.74
v (km s^{-1})	156	210
$\tau^{(\alpha)}$	0.97	0.07
$D_{\rm eff}$ (km)	40 000	3600
f (%)	71	7

UVCS and LASCO data were available (points P1 and P2; see Figs. 1 and 2). The plasma parameters obtained for the two points are listed in the top part of Table 1, together with the statistical uncertainties that have been derived from the Gaussian-fit parameters.

For these two points, the code was iteratively run taking the measured quantities as initial input parameters and the gas pressure as a free parameter, until the computed intensities of Lyα and Lyβ lines matched the observed values. The additional information on the electron column density derived with LASCO was used to constrain the model, so that it was possible to derive even the effective prominence thickness, $D_{\rm eff}$. Calculations in Paper I were originally performed using the Lyα and Lyβ incident radiation profiles reported in Gouttebroze et al. (1993); they were obtained from solar disk measurements performed in 1976 (i.e., around solar activity minimum) with the OSO-8/LPSP instrument (see Sect. 5.2 of Paper I). However, for the purposes of this work and in order to explore a different choice of the incident radiation profiles, the detailed modeling in points P1 and P2 has been repeated using the more recent Lyα and Lyβ line profiles measured on the solar disk with SOHO/SUMER in May 2000 and reported in Lemaire et al. (2015; see the details in the next section). The final model parameters are listed in the second part of Table 1; they only slightly differ from the values reported in Paper I.

In addition to the general results concerning the plasma thermodynamics that have been discussed in Paper I and Paper II, we recall here that the resulting effective thickness was combined with the observed thickness estimated from LASCO-C2 images, $D = 56\,000$ km, to infer the prominence LOS filling factor in the two points. This was done by implicitly assuming an irregularity factor $X = 1$ (so that $f = D_{\rm eff}/D$; see Paper I), because the 1D-slab prominence model assumes that all the plasma parameters are uniform along the LOS. The filling factor obtained in this way is lower than one in both points. This suggests that the prominence most likely undergoes fragmentation during its expansion; for instance, in point P2, where $f \ll 1$, only a very small portion of the LOS contributes to the Lyman emission observed by UVCS. This supports the interpretation that in the southern prominence leg, which is moving and expanding at higher velocity, the emitting plasma may be more rarefied and distributed on spatial scales smaller than the length D estimated from the visible light.

4. Analysis methods

We aim here to test a partially independent technique to infer the prominence LOS filling factor, based on UVCS observations of Lyα and Lyβ emission lines, and to check the consistency of the results against the model values presented in Paper I. The general approach is to use the results of the detailed modeling of prominence points P1 and P2 (i.e., hydrogen kinetic and effective temperatures and outflow velocities) to (1) evaluate the expected intensities of the radiative and collisional components of one or both of the hydrogen Lyman lines in the two points, according to the formalism described in Sect. 2, and (2) estimate the filling factor from the comparison with the measured intensities. All the other quantities are constrained by the observations or reasonably assumed.

4.1. Incident radiation and Doppler-dimming calculations

As anticipated in the previous section, the incident radiation profiles of the Lyα and Lyβ lines adopted for our calculations were derived from the high-resolution spectral irradiance profiles measured on the solar disk with SOHO/SUMER on May 20, 2000 (see Lemaire et al. 2015); from the several measurements reported in that paper, spanning most part of solar cycle 23, we selected those closest to the date of our event. Using the same approach as we described in Paper I, the Lyα profile was renormalized to match the actual total integrated intensity at the time of the event, $I_\odot^{(\alpha)} = 1.29 \times 10^5$ erg cm^{-2} s^{-1} sr^{-1}, derived from the Lyα flux at Earth measured with SOLSTICE; the Lyβ profile was renormalized according to the results reported by Lemaire et al. (2015) on the variations of the Lyα to Lyβ intensity ratio during the solar cycle, giving $I_\odot^{(\beta)} \simeq 0.022 \cdot I_\odot^{(\alpha)}$. The line profiles are shown in Fig. 3.

The Doppler-dimming factor is calculated assuming a Gaussian absorption profile with an FWHM corresponding to the effective temperatures in points P1 and P2 derived from the model and listed in Table 1. The incident radiation profile was redshifted according to the outflow velocities (v) reported in the Table. We recall that these velocity values are lower than the POS component of the prominence speed measured with LASCO because they were required to reach the best agreement between the observed and the synthesized Lyα and Lyβ intensities. On the other hand, as described in Paper I, the

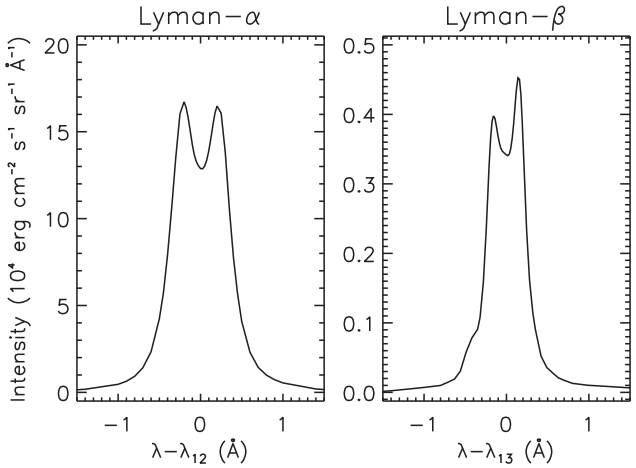

Fig. 3. Solar disk Lyα and Lyβ spectral profiles derived from SOHO/SUMER measurements (see Lemaire et al. 2015).

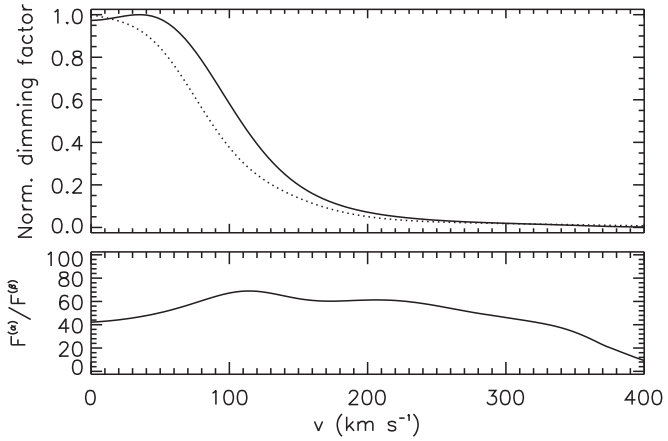

Fig. 4. Normalized Doppler-dimming factor of the hydrogen Lyα (*top panel*, solid line) and Lyβ (dotted line) lines, calculated for the representative temperature of 10^5 K, and ratio of two factors (*bottom panel*), as functions of the plasma outflow velocity.

analysis of UVCS O VI data has shown that the v_{POS} estimated from LASCO images is most probably an overestimate of the real outflow velocity due to the prominence acceleration in the first phases of its evolution.

Figure 4 shows, as an example, the dimming factors $F^{(\alpha)}$ and $F^{(\beta)}$ of the Lyα and Lyβ lines, respectively, computed as functions of the outflow velocity for the representative temperature of 10^5 K, together with the ratio $F^{(\alpha)}/F^{(\beta)}$. It is worth noting that the Lyα dimming factor is not a monotonically decreasing function of the outflow velocity, at variance with the typical behavior obtained for coronal plasma (see for a comparison Kohl & Withbroe 1982). This is caused by the relatively narrow absorption profile, in this case relevant to temperatures typical of prominences, making the Doppler dimming much more sensitive to the shape of the incident radiation profile. The slight increase in the dimming factor that occurs for velocities from zero to ~40 km s^{-1} is due to the transition from the central dip to the peak of the disk profile, which leads to a "pumping" of the radiative component of the line that is expected to be enhanced by the plasma flow in this velocity range.

4.2. Collisional rates and ionization balance

The collisional excitation coefficients for Lyα and Lyβ transitions were numerically computed using the five-level hydrogen model atom with continuum described in Gouttebroze et al. (1993). The resulting collisional rates for the Lyα (q_{12}) are plotted in Fig. 5 versus temperature.

It is interesting to compare these rates with an analytical approximation that is widely used for typical coronal lines, as found, for instance, in Mewe (1972):

$$q_{ij}(T) \simeq 2.73 \times 10^{-15} \frac{f_{ij} \cdot g}{E_{ij}\, T^{1/2}} \exp\left(-\frac{E_{ij}}{k_B T}\right), \qquad (12)$$

where f_{ij} is the absorption oscillator strength for the transition, g the average electron-impact Gaunt factor, $E_{ij} = hc/\lambda_{ij}$ the transition energy, and q_{ij} is in cgs units. At the temperatures characteristic of the prominence plasma (~10^5 K), the collisional rates computed with this theoretical approximation are a factor of ~2 higher than the coefficients computed numerically with the five-level hydrogen atom model (see Fig. 5). We note that the collisional coefficient for the Lyβ transition is in both cases about 20% of that relevant to the Lyα above 10^5 K.

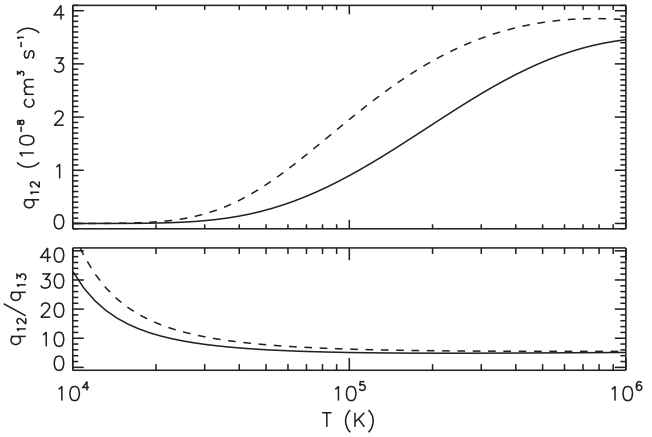

Fig. 5. Collisional coefficients for the Lyα transition (*top panel*) and ratio of the Lyα-to-Lyβ coefficients (*bottom panel*), computed as functions of the temperature using the five-level hydrogen model atom with continuum described in Gouttebroze et al. (1993; solid lines) and the theoretical approximation (given by Eq. (12); dashed lines).

The hydrogen ionization fraction $R(T)$ is taken from the ionization equilibrium of Arnaud & Rothenflug (1985, provided by the CHIANTI atomic database, version 7). Although this is a simplification, because plasma in expanding prominences can be out of ionization equilibrium, we checked that the ionization degree computed by the numerical code used in Paper I agreed reasonably well with that provided by Arnaud & Rothenflug (1985).

5. Results

According to Eq. (10), it is necessary to separate the radiative and collisional components of one of the two Lyman lines in order to derive the prominence plasma filling factor. To do this, we followed two different methods, with different degrees of approximation. In the first, we used the intensities of the Lyα and Lyβ lines to separate the radiative and collisional components of each line; in the second method, we evaluated the two components of the Lyα intensity in points P1 and P2 as a function of the filling factor, using Eqs. (6) and (8), and determined the best value of f from the comparison with the measured intensity.

Table 2. Resulting radiative and collisional components.

		P1		P2	
		Lyα	Lyβ	Lyα	Lyβ
First method	$I_{\rm rad}$	212.5	0.43	10.0	0.02
	$I_{\rm col}$	3.5	0.47	2.5	0.38
Second method	$I_{\rm rad}$	183.2	0.55	5.6	0.01
	$I_{\rm col}$	32.8	0.35	6.9	0.39

5.1. First method

Given the total intensities of both Lyα and Lyβ lines, the collisional and radiative components can be easily separated according to Fineschi & Romoli (1994) using the ratios

$$R_{\rm col} \equiv \frac{I^{(\alpha)}_{\rm col}}{I^{(\beta)}_{\rm col}} = \frac{\lambda_{13}\, b_{12}\, q_{12}}{\lambda_{12}\, b_{13}\, q_{13}} \simeq 0.96 \cdot \frac{q_{12}}{q_{13}} \tag{13}$$

and

$$R_{\rm rad} \equiv \frac{I^{(\alpha)}_{\rm rad}}{I^{(\beta)}_{\rm rad}} = \frac{B_{12}\, \lambda_{12}\, b_{12}\, F^{(\alpha)}}{B_{13}\, \lambda_{13}\, b_{13}\, F^{(\beta)}} \simeq 8.4 \cdot \frac{F^{(\alpha)}}{F^{(\beta)}}, \tag{14}$$

where all quantities are known or can be estimated as explained in the previous sections. Using these relationships together with Eqs. (1), (10) can be rewritten as

$$f = K(T) \cdot \frac{N_{\rm e}^2}{D} \cdot \left[I^{(\alpha)}_{\rm tot} - R_{\rm rad}(v) \cdot \frac{I^{(\alpha)}_{\rm tot} - R_{\rm col} I^{(\beta)}_{\rm tot}}{R_{\rm rad}(v) - R_{\rm col}} \right]^{-1} . \tag{15}$$

The advantage of using the above expressions is that the separation of the radiative and collisional components of the two lines is based on relative ratios that are less sensitive to the overall assumptions (e.g., they are independent of the hydrogen ionization degree, the electron density, and the geometry of the resonant scattering); however, the reliance of the ratios on the collisional coefficients and the incident radiation profiles through the dimming factors is still a potential source of uncertainty.

According to the previous equations, the radiative component of the Lyα line is ~98% of the total intensity in point P1 and ~80% in point P2 (see Table 2). Although the resonantly scattered component may be dimmed by more than 50% at velocities above 100 km s^{-1} (see Fig. 4 and, e.g., the discussion in Kohl & Withbroe 1982), its contribution is still overwhelming in both points. The Lyβ line, conversely, is more collisional, since the collisional component is ~50% of the observed intensity in P1 and up to ~95% in P2 (see Table 2). This is in agreement with the general evidence that in high-density coronal structures, such as prominences or streamers, the Lyα line is essentially radiatively formed, but the Lyβ line is more collisionally driven (Labrosse et al. 2006; Vial & Chane-Yook 2016).

The resulting filling factors are $f = (74 \pm 21)\%$ in point P1 and $f = (5 \pm 1)\%$ in point P2. The uncertainties have been estimated from the measurement errors, in particular from the UVCS intensity errors. We point out that actual uncertainties on the results may be larger, especially because of the large uncertainty affecting the column density measurement, which can hardly be quantified, however. As we also show in the following sections, small changes in the outflow velocity and kinetic temperature that we assumed for the calculations may dominate the uncertainty and affect the resulting filling factor as well.

In both points we obtain a satisfactory agreement with the results from the non-LTE model. This is interesting and shows that even the simple method described here is able to give results similar to those provided by the more robust non-LTE modeling when the necessary plasma parameters are well constrained from the observations. However, it must be emphasized that our approach is based on relationships that are strictly valid only for optically thin lines ($\tau < 1$), a condition that is usually satisfied in the corona but not necessarily in erupting prominences, where densities are higher and temperatures lower. This nice agreement is then at least in part a consequence of the mild optical depth characterizing the two selected points (see Table 1), compared to typical τ values derived at the center of the Lyα and Lyβ lines in quiescent prominences (e.g., Gouttebroze et al. 1993).

The above results were obtained using the numerically computed collisional rates; when the theoretical approximation of Eq. (12) is used instead, an unrealistic filling factor $f \gg 1$ is obtained in point P1, while in point P2 we obtain $f = (18 \pm 8)\%$, which is consistent with the model value only within 2σ.

5.2. Second method

We also tried to estimate the prominence filling factor using the intensity of the Lyα line alone, in combination with the results obtained from LASCO-C2 data. This attempt was motivated by our wish to check the reliability of this method in the perspective of applying it to the future data delivered by the Metis coronagraph (see Antonucci et al. 2012) on board the Solar Orbiter spacecraft (see Müller et al. 2013) and other similar instruments such as the LST on board the ASO-S chineese mission (see Li 2015). In particular, Metis will for the first time provide simultaneous and cospatial Lyα and visible-light images of the solar corona above ~1.6 $R_\odot$ in the whole instrument FOV, offering interesting opportunities for the study of erupting prominences. We remark, however, that Metis will lack spectroscopic observations, therefore additional assumptions on the effective and kinetic temperatures, derived in this work from UVCS observations, will be required. Nevertheless, it will provide high-resolution, high-cadence image sequences that will allow a better measurement of the outflow speed to within the uncertainties related to the direction relative to the POS, which can be estimated from considerations on the position of the eruption.

The radiative component of the Lyα line can be directly estimated using Eq. (6) with the plasma parameters listed in Table 1; the collisional component can be evaluated instead as a function of the filling factor using Eq. (8). Adding the two gives the total expected intensity versus filling factor; the resulting curves for the two points are plotted in Fig. 6.

It is evident that for both points the filling factor derived from the comparison of the expected intensity with the measured one is lower than the prominence model value. We obtain $f = (7.3 \pm 0.2)\%$ in point P1 (against 71%) and $f = (1.5 \pm 0.2)\%$ in point P2 (against 7%). The radiative component of the Lyα line is ~85% of the total observed intensity in point P1 and ~45% in point P2 (see Table 2), that is, the predicted collisional component is significantly greater than that estimated with the Lyα/Lyβ ratio because Eq. (6) most probably underestimates the intensity of the radiative component. This could explain why the filling factor is ~10 times lower than the model value in point P1 and ~5 times lower in point P2. We note that the filling factor would increase by a factor of ~3 if the collisional rates were computed using Eq. (12); nevertheless, the results would be still lower than the model values.

As a further test, we performed the same calculation using the Lyβ line. In point P1 we obtain $f \approx 1$; conversely, in point P2 we obtain $f = (5 \pm 1)\%$ using the collisional coefficients

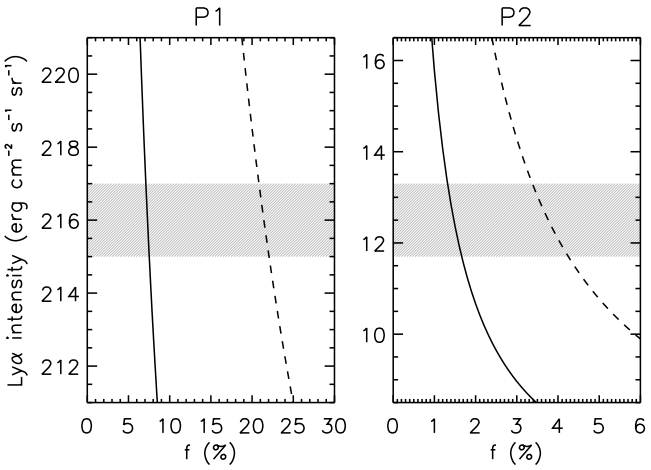

Fig. 6. Total Lyα intensity computed as a function of the LOS plasma filling factor using the method described in Sect. 5.2 with the numerical (solid lines) and theoretical (using Eq. (12); dashed line) collisional coefficients for the computation of the collisional rates. The gray bands, plotted for reference purposes, mark the uncertainty range around the total integrated line intensities measured with UVCS.

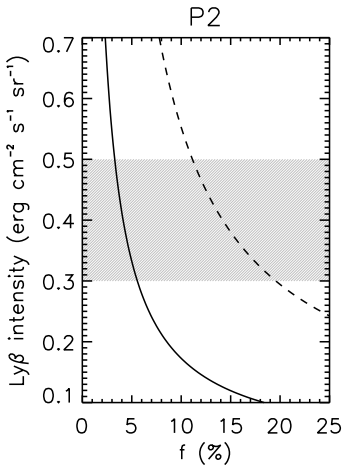

Fig. 7. Same as in Fig. 6 for the Lyβ intensity computed in point P2.

computed numerically (see Fig. 7). Given the large uncertainties affecting the intensity of this line (about 30%, see Table 1), the rather acceptable agreement with the model achieved in point P2 is interesting. Two circumstances probably correspond to this result: (1) the collisional component of the Lyβ intensity is dominant in point P2 (~95% of the total intensity, in agreement with the value obtained with the first method; see Table 2), and (2) opacity effects in the Lyβ line are very negligible in this point because $\tau^{(\alpha)} \ll 1$, and in general, $\tau^{(\beta)} < \tau^{(\alpha)}$ (see, e.g., Gouttebroze et al. 1993).

5.3. Exploration of the parameter space

In the previous sections we have used the measured Lyman line intensities and the visible-light brightness together with the plasma parameters (v and T) derived from the non-LTE prominence model to check the consistency of the methods in estimating the prominence plasma filling factor. However, it is interesting to explore the parameter space more extensively in order to collect information on the possible uncertainties of the computation and on the optimum ranges for the plasma parameter values.

According to the method described in Sect. 5.1, Eq. (15) can be used to compute the filling factor as a function of both outflow velocity and kinetic temperature, with the other plasma quantities (effective temperature and electron column density) fixed by the observations. It is possible, therefore, to obtain 2D maps of the filling factor required to reproduce simultaneously the observed Lyα and Lyβ intensities in the (v, T) space.

We limited our exploration to the velocity range between 0 and 300 km s^{-1}, because, as found in Paper I, the prominence velocity derived from LASCO images ($v_{\rm POS} \simeq 300$ km s^{-1}) can be regarded as an upper limit to the real plasma outflow velocity. As for the kinetic temperature, we considered the range between $10^{4.5}$ and 10^5 K, where the upper limit is constrained by the observed effective temperatures ($T_{\rm eff} \lesssim 10^5$ K) and the lower limit has been reasonably assumed according to the results of our analysis. Figure 8 shows the resulting filling factor maps for the two points.

The plots show that the dependence of the filling factor on the plasma parameters is quite moderate. In the explored

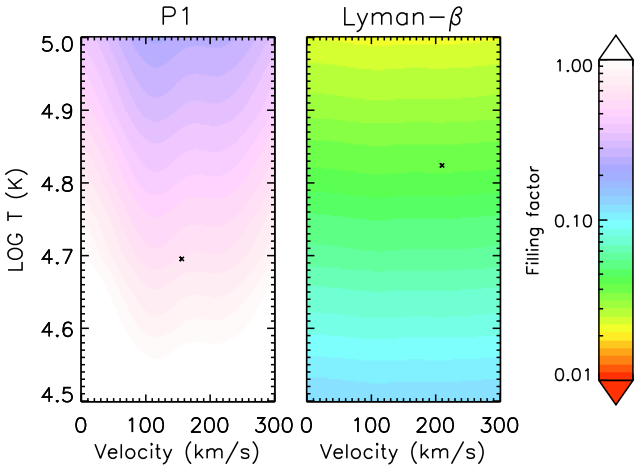

Fig. 8. 2D maps of the filling factor obtained using Eq. (15) as a function of outflow velocity and kinetic temperature for point P1 (*left panel*) and P2 (*right panel*). The crosses mark the points in the (v, T) plane corresponding to the non-LTE-model results.

domain, f varies between ~20–100% in point P1 and between ~2 and 12% in point P2. This ranges give a first-order indication of the possible values of the prominence plasma filling factor that are consistent with the non-LTE model results. We note that the dependence on the outflow velocity is weaker than that on the kinetic temperature, which we find to be the most critical parameter. Interestingly, in point P2, the filling factor appears to be practically independent on the outflow velocity, and this is in agreement with the fact that in that point the line intensity is dominated by the collisional component.

These results place important constraints on the use of the method described in Sect. 5.1; using Eq. (15), it is possible to derive an accurate estimate of the filling factor (or at least, to restrict the possible value range for this parameter) only if the plasma outflow velocity, and especially the kinetic temperature, are rather well constrained by the observations. For instance, we estimated that an uncertainty $\Delta \log T = 0.1$ corresponds to an average uncertainty of ~40% in the resulting filling factor.

Alternatively, using Eqs. (6) and (8), the intensities of the Lyα and Lyβ lines can be calculated separately for each set of parameters (v, T, f), meaning that the parameter space is 3D in this case. For both lines, the region of the parameter space where the computed intensity matches the observed one is therefore a

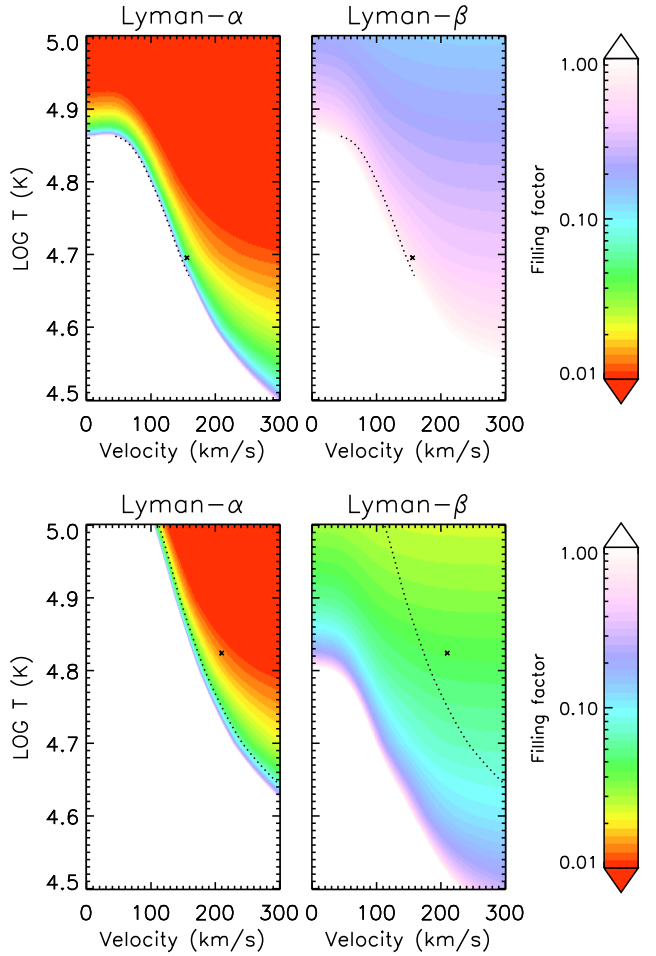

Fig. 9. Filling factor maps obtained with combination of Eqs. (6) and (8) as a function of outflow velocity and kinetic temperature. For each pair (v, T), the maps give the corresponding f values required to reproduce the intensities of the Lyα (*left panels*) and Lyβ (*right panels*) lines measured in point P1 (*top panels*) and P2 (*bottom panels*), respectively. The dotted line identifies the region of the parameter space (projected onto the $[v, T]$ plane) where intensities of both lines are matched simultaneously. As in Fig. 8, the crosses mark the points corresponding to the non-LTE-model results.

2D surface that can be represented as a color gradient map projected in the (v, T) plane (see Fig. 9). The intersection of the two surfaces identifies the region where the intensity of both lines can be reproduced at once with a single set of parameters; this region is marked with the dotted line in the plots of Fig. 9.

The general trend is that the filling factor rapidly exceeds 100% for decreasing values of both outflow velocity and kinetic temperature; variations are steeper for the Lyα line, whose intensity is more sensitive to the outflow velocity due to Doppler dimming. In point P1, the region of the parameter space where simultaneous matching of the measured intensities is achieved is limited, so that it is possibile to reproduce the observed Lyα and Lyβ intensities only for velocities between 40 and 160 km s^{-1} and temperatures between $10^{4.67}$ and $10^{4.87}$ K; the filling factor in the intersection region varies between 54 and 94%. It is worth noting that the point representative of the non-LTE model (marked with a cross in the plots) lies outside this region, as expected on the basis of the results obtained in Sect. 5.2. Although the approximate approach described there is not accurate at reproducing the model results when the two Lyman lines are considered separately, when they are combined, it is possible to obtain a rough indication on the best ranges for the prominence plasma parameters that are in good agreement with the results of the detailed prominence modeling.

The situation is similar for point P2, for which, nevertheless, the parameter space region where the Lyα and Lyβ line intensities can be reproduced at once is not limited. Therefore, the plasma parameters can only be constrained by the observations in this case, which suggest temperatures below $\sim 10^{4.9}$ K and velocities below $\sim$300 km s^{-1}. In this domain, the filling factor required to match both line intensities varies between 2 and 7%. This again agrees quite well with the non-LTE model results.

6. Discussion and conclusions

We combined cospatial and cotemporal visible-light and neutral hydrogen Lyα and Lyβ observations to obtain information on the LOS filling factor of the plasma embedded in an erupting prominence detected in the core of a CME. The methods we presented are based on the comparison of the Lyα and Lyβ line intensities measured by UVCS with those evaluated using theoretical approximations for resonant scattering and collisional excitation, using the electron column density inferred from LASCO-C2 total-brightness data, and constraining all the other quantities from the observations or properly assuming them. In particular, we exploited the results of the detailed non-LTE prominence modeling described in Paper I to test the validity of these techniques. The model provided us with the hydrogen kinetic temperature, microturbulence (and, therefore, the effective Lyα and Lyβ absorption line widths), and plasma flow velocity in two prominence points where simultaneous and cospatial UVCS and LASCO data were available. We derived the plasma filling factor with two slightly different methods and compared the results with the values obtained from the model in order to check their reliability.

Our results show that the derived filling factors are satisfactorily consistent with the model values when the intensities of the Lyα and Lyβ lines are used together to distinguish the radiative and collisional components of each line, according to the technique described by Fineschi & Romoli (1994). Since only the collisional component explicitly depends on the filling factor, separating the two components is crucial. The use of two lines from the same atomic species, in our case, the hydrogen Lyman lines, minimizes the uncertainties that are due to the ionization balance, electron density, and element abundance, and reduces the effects relevant to the Doppler dimming and collisional excitation.

When the two lines are considered separately, the results are not consistent with the model, or there is only a marginal agreement in the prominence point where opacity effects are more negligible (i.e., point P2) because of the lower plasma optical depth. On the one hand, this is a consequence of the fact that the approximate relationships we used for the theoretical computation of the line intensities are very sensitive to the Doppler dimming coefficient, collisional rates, and hydrogen neutral fraction, thus the uncertainties on these terms may dominate depending on the predominant transition excitation regime (radiative/collisional). On the other hand, the formalism described in Sect. 2 is strictly valid for UV emission in optically thin coronal lines. As demonstrated in Paper I, a significant fraction of prominence points (between one-third and one-half) was found to be optically thick in Lyα, therefore the limitations of the results obtained when applying this technique to prominence observations need to be considered. The method described in Sect. 5.2 may then be a better diagnostic for the outflow

velocity (see, e.g., Dolei et al. 2018; Bemporad 2017) or the plasma temperature (see Susino & Bemporad 2016) than for the filling factor.

The most critical assumptions of our analysis are relevant to the incident radiation intensity and profile, the flow velocity, and the plasma temperature. The intensity of the chromospheric Lyα and Lyβ radiation can be constrained by Lyα irradiance measurements, while line profiles can be provided by solar disk spectral measurements. The solar activity, either on global scales during the solar cycle (see Tobiska et al. 1997) or locally in active regions, affects the intensities and the spectral profiles of both lines. For instance, the Lyα flux may increase by a factor of ~1.5 between solar minimum and maximum, and the Lyβ by a factor slightly larger (see Woods et al. 2000; Lemaire et al. 2015). In addition, there is also evidence of the variability of the Lyα/Lyβ line-intensity ratio, depending on the predominant magnetic configuration (quiet Sun vs. active region) of the portion of the disk that illuminates the prominence (see, e.g., Tian et al. 2009, and references therein). Therefore, the particular assumption made for the line profiles can affect the results to a large extent, the magnitude of these effects being related to the flow velocity through the Doppler-dimming term.

The radial component of the flow velocity can be roughly estimated from the the visible-light images, but this determination is affected by projection effects. As we showed in Paper I, the POS component of the prominence velocity estimated from LASCO-C2 images is significantly larger than the radial component required to reproduce the observed intensities of the Lyα and Lyβ lines. In our specific case, however, we find that the ratio of the dimming factors $F^{(\alpha)}/F^{(\beta)}$ slowly decreases, within ~30%, in the velocity range between 100 and 300 km s^{-1} (see Fig. 4), so that our final results are mildly dependent on the flow velocity when the method described in Sect. 5.1 is used.

The knowledge of the hydrogen kinetic plasma temperature is fundamental to reliably evaluate the Lyman line intensities, and, in turn, the filling factor, especially in the temperature range typical of prominences, where collisional rates and ionization balance can vary by orders of magnitude. The kinetic temperature is related to the effective temperature through the (unknown) nonthermal motions. The sensitivity of our methods on the effective temperature, which constrains the width of the absorption profile, is quite weak: we checked that a variation of a factor of 2 on this parameter causes a variation no larger than ~15% in the filling factor values. Conversely, the dependence on the kinetic temperature can be stronger, as evidenced by the exploration of the parameter space described in Sect. 5.3, because this parameter affects both the collisional coefficients and the ionization fraction.

Unlike the effective temperature, which can be constrained by the spectroscopic observations, the kinetic temperature must be inferred by means of assumptions on the nonthermal plasma motions that broaden the line profiles, such as the microturbulence. In Paper I, we assumed the microturbulent velocity to be a constant fraction of the sound speed (i.e., proportional to the square root of the plasma temperature), implying a precise relationship between kinetic and effective temperatures (see Appendix A of Paper I). Even if this hypothesis is plausible (according to Parenti & Vial 2007) and can be used for a first, approximate estimate of the microturbulent velocity, a detailed modeling of the hydrogen Lyα and C III 977.02 Å lines observed with UVCS (see Paper II) shows that if these lines are used together to separate the kinetic temperature and the microturbulence from the line widths, the resulting microturbulent velocity in the prominence is not simply correlated to the kinetic temperature, but it is rather constant within the uncertainties (with values around 25 km s^{-1}). This makes it harder to relate the kinetic plasma temperature to the effective temperature.

These considerations underline that our results are significant as far as all the assumptions can be considered reasonable. However, we also showed that a combination of the two methods might be used not only to derive a first-order estimate of the prominence plasma filling factor, but also to provide an approximate, initial guess of the plasma parameters, which might in turn be used to set up a more detailed modeling. We point out that the use of simultaneous LASCO-C2 and UVCS data has restricted our analysis to only two prominence points because of the low temporal cadence of the C2 images and the limited spatial FOV of UVCS. Therefore, additional investigation by considering, for instance, a number of eruptive prominence events observed in the visible light and UV would be useful to further test the techniques we presented.

Acknowledgements. Support from the Agenzia Spaziale Italiana through contract ASI/INAF No. I/013/12/0-1 is kindly acknowledged by RS and AB. SJ and PH acknowledge the support from the grant of the Czech Funding Agency No. 16-18495S. SJ also acknowledges financial support from the Slovenian Research Agency No. P1-0188. We also thank the referee for their valuable suggestions that helped us to greatly improve the paper.

References

Akmal, A., Raymond, J. C., Vourlidas, A., et al. 2001, ApJ, 553, 922
Allen, C. W. 1963, in IAU Symp., ed. J. W. Evans, The Solar Corona, 16, 1
Antonucci, E., Fineschi, S., Naletto, G., et al. 2012, in Proc. SPIE, Space Telescopes and Instrumentation 2012: Ultraviolet to Gamma Ray, 8443, 844309
Arnaud, M., & Rothenflug, R. 1985, A&AS, 60, 425
Bemporad, A. 2017, ApJ, 846, 86
Berger, T. 2014, in IAU Symp., ed. B. Schmieder, J.-M. Malherbe, & S. T. Wu, Nature of Prominences and their Role in Space Weather, 300, 15
Chen, P. F. 2011, Liv. Rev. Sol. Phys., 8, 1
Ciaravella, A., Raymond, J. C., van Ballegooijen, A., et al. 2003, ApJ, 597, 1118
Dolei, S., Susino, R., Sasso, C., et al. 2018, A&A, 612, A84
Fineschi, S., & Romoli, M. 1994, Space Sci. Rev., 70, 353
Gouttebroze, P., Heinzel, P., & Vial, J. C. 1993, A&AS, 99, 513
Habbal, S. R., Druckmüller, M., Morgan, H., et al. 2010, ApJ, 719, 1362
Heinzel, P., Susino, R., Jejčič, S., Bemporad, A., & Anzer, U. 2016, A&A, 589, A128 (Paper I)
Jejčič, S., Susino, R., Heinzel, P., et al. 2017, A&A, 607, A80 (Paper II)
Kohl, J. L., & Withbroe, G. L. 1982, ApJ, 256, 263
Labrosse, N. 2015, in Astrophysics and Space Science Library, ed. J.-C. Vial & O. Engvold, Solar Prominences, 415, 131
Labrosse, N., Li, X., & Li, B. 2006, A&A, 455, 719
Labrosse, N., Heinzel, P., Vial, J.-C., et al. 2010, Space Sci. Rev., 151, 243
Lemaire, P., Vial, J.-C., Curdt, W., Schühle, U., & Wilhelm, K. 2015, A&A, 581, A26
Li, H. 2015, IAU Gen. Assembly, 22, 2232958
Mackay, D. H., Karpen, J. T., Ballester, J. L., Schmieder, B., & Aulanier, G. 2010, Space Sci. Rev., 151, 333
Mariska, J. T., Doschek, G. A., & Feldman, U. 1979, ApJ, 232, 929
Mewe, R. 1972, A&A, 20, 215
Müller, D., Marsden, R. G., St. Cyr, O. C., & Gilbert, H. R. 2013, Sol. Phys, 285, 25
Noci, G., Kohl, J. L., & Withbroe, G. L. 1987, ApJ, 315, 706
Parenti, S. 2015, in Astrophysics and Space Science Library, ed. J.-C. Vial & O. Engvold, Solar Prominences, 415, 61
Parenti, S., & Vial, J.-C. 2007, A&A, 469, 1109
Patsourakos, S., & Vial, J.-C. 2002, Sol. Phys., 208, 253
Romoli, M., & Fineschi, S. 1994, Space Sci. Rev., 70, 359
Susino, R., & Bemporad, A. 2016, ApJ, 830, 58
Tian, H., Curdt, W., Marsch, E., & Schühle, U. 2009, A&A, 504, 239
Tobiska, W. K., Pryor, W. R., & Ajello, J. M. 1997, Geophys. Res. Lett., 24, 1123
Vial, J.-C., & Engvold, O., eds. 2015, Astrophysics and Space Science Library, Solar Prominences, 415
Vial, J.-C., & Chane-Yook, M. 2016, Sol. Phys., 291, 3549
Vourlidas, A., Subramanian, P., Dere, K. P., & Howard, R. A. 2000, ApJ, 534, 456
Webb, D. F., & Howard, T. A. 2012, Liv. Rev. Sol. Phys., 9, 3
Woods, T. N., Tobiska, W. K., Rottman, G. J., & Worden, J. R. 2000, Geophys. Res, 105, 27195